Characterization of optical-surface-imaging-based spirometry for respiratory surrogating in radiotherapy

Guang Li[a)]
Department of Medical Physics, Memorial Sloan Kettering Cancer Center, New York, New York 10065

Jie Wei
Department of Computer Science, City College of New York, New York, New York 10031

Hailiang Huang, Qing Chen, Carl P. Gaebler, Tiffany Lin, and Amy Yuan
Department of Medical Physics, Memorial Sloan Kettering Cancer Center, New York, New York 10065

Andreas Rimner
Department of Radiation Oncology, Memorial Sloan Kettering Cancer Center, New York, New York 10065

James Mechalakos
Department of Medical Physics, Memorial Sloan Kettering Cancer Center, New York, New York 10065

(Received 16 May 2015; revised 18 January 2016; accepted for publication 29 January 2016; published 23 February 2016)

Purpose: To provide a comprehensive characterization of a novel respiratory surrogate that uses optical surface imaging (OSI) for accurate tidal volume (TV) measurement, dynamic airflow (TV′) calculation, and quantitative breathing pattern (BP) estimation during free breathing (FB), belly breathing (BB), chest breathing (CB), and breath hold (BH).
Methods: Optical surface imaging, which captures all respiration-induced torso surface motion, was applied to measure respiratory TV, TV′, and BP in three common breathing patterns. Eleven healthy volunteers participated in breathing experiments with concurrent OSI-based and conventional spirometric measurements under an institutional review board approved protocol. This OSI-based technique measures dynamic TV from torso volume change ($\Delta V_{\text{torso}} = \text{TV}$) in reference to full exhalation and airflow ($\text{TV}' = d\text{TV}/dt$). Volume conservation, excluding exchanging air, was applied for OSI-based measurements under negligible pleural pressure variation in FB, BB, and CB. To demonstrate volume conservation, a constant TV was measured during BH while the chest and belly are moving ("pretended" respiration). To assess the accuracy of OSI-based spirometry, a conventional spirometer was used as the standard for both TV and TV′. Using OSI, BP was measured as $\text{BP}^{\text{OSI}} = \Delta V_{\text{chest}}/\Delta V_{\text{torso}}$ and BP can be visualized using $\text{BP}^{\text{SHI}} = \text{SHI}_{\text{chest}}/(\text{SHI}_{\text{chest}} + \text{SHI}_{\text{belly}})$, where surface height index (SHI) is defined as the mean vertical distance within a region of interest on the torso surface. A software tool was developed for OSI image processing, volume calculation, and BP visualization, and another tool was implemented for data acquisition using a Bernoulli-type spirometer.
Results: The accuracy of the OSI-based spirometry is $-21 \pm 33\ \text{cm}^3$ or $-3.5\% \pm 6.3\%$ averaged from 11 volunteers with 76 ± 28 breathing cycles on average in FB. Breathing variations between two separate acquisitions with approximate 30-min intervals are substantial: $-1\% \pm 34\%$ (ranging from -64% to 40%) in TV, $4\% \pm 20\%$ (ranging from -50% to 26%) in breathing period (T), and $-1\% \pm 34\%$ (ranging from -49% to 44%) in BP. The airflow accuracy and variation (between two exercises) are $-1 \pm 54\ \text{cm}^3/\text{s}$ and $-5\% \pm 30\%$, respectively. The slope of linear regression between OSI–TV and spirometric TV is 0.93 ($R^2 = 0.95$) for FB, 0.96 ($R^2 = 0.98$) for BB, and 0.95 ($R^2 = 0.95$) for CB. The correlation between the two spirometric measurements is 0.98 ± 0.01. BP increases from BB, FB to CB, while TV increases from FB, BB, to CB. Under BH, 4% volume variation (range) on average was observed.
Conclusions: The OSI-based technique provides an accurate measurement of tidal volume, airflow rate, and breathing pattern; all affect internal organ motion. This technique can be applied to various breathing patterns, including FB, BB, and CB. Substantial breathing irregularities and irreproducibility were observed and quantified with the OSI-based technique. These breathing parameters are useful to quantify breathing conditions, which could be used for effective tumor motion predictions.
 [http://dx.doi.org/10.1118/1.4941951]

Key words: respiratory motion, breathing tidal volume, optical surface imaging

1. INTRODUCTION

In radiation therapy of lung, liver, and pancreatic cancer, especially stereotactic body radiation therapy (SBRT), breathing irregularities are likely one of the major obstacles that prevents external respiratory surrogates from producing reliable tumor motion information.[1–4] Almost all existing external motion surrogates rely on a linear internal–external correlation,

which may degrade or even break down due to patient breathing irregularities.[5–7] There are three major types of external surrogates: (1) infrared reflectors/emitters placed on the chest or upper abdomen, (2) respiratory bellows wrapped around the abdomen with a tension sensor, and (3) breathing tidal volume (TV) measured with a spirometer. Recently, optical surface imaging (OSI) has been studied as a markerless external surrogate using a local region of interest,[8–10] but is still based on the external–internal correlation, which requires initial calibration and periodic verification using an internal surrogate to ensure a reliable prediction of tumor motion.[11–13] The correlation-based techniques suffer from several major shortcomings, including daily fiducial placement uncertainty, location dependency, requirement for internal markers, incapability of detecting breathing pattern[14–16] (that determines the contributions from the diaphragm and intercostals), as well as poor reliability due to breathing irregularities: the correlation-based model[17] may need to be rebuilt multiple times during treatment.

Quantitatively, the major uncertainties in the correlation-based prediction include: (1) the statistical relationship may vary, degrade, or break down as patient breathing behavior changes (irregularities), (2) the linear relationship is only an approximation of the nonlinear behavior such as respiratory hysteresis and phase shift in tumor motion, and (3) local external surrogates do not provide a comprehensive view of external motions, and therefore, it is almost impossible to establish a physical relationship. Biomechanical approaches to the external–internal relationships have been applied. An early example is the so-called 5D model,[18,19] which distinguishes itself from the correlation-based model by relating to biomechanical modeling.[20] This model suggests that tumor motion is a function of five physical parameters: tumor location (x, y, z), TV, and airflow (TV′). However, establishment of the model requires training with the use of patient-specific data, such as 4DCT imaging and spirometric measurement. Fundamental studies, based on Hooke's law, using finite element analysis have predicted respiratory lung motion with sufficient accuracy. However, the associated computation is too prohibitively expensive to yield real-time performance.[21–24] In addition, dynamic boundary conditions of the lung or body would be required for tumor motion prediction. Recently, an attempt to establish a physical model has been reported based on physical relationships between external and internal motion.[14,15,25] This physical approach intends to predict tumor motion under breathing irregularities, which can be measured and updated with OSI-based spirometry[16] in reference to the initial 4DCT simulation.

We hereby extend our previous study[16] to provide a comprehensive validation of the OSI-based approach using 11 human subjects' data under an institutional review board (IRB)-approved protocol study. With sub-millimeter (0.2 mm) spatial accuracy,[8,26,27] OSI can produce highly accurate surface images, which are essential for precise volume calculation. With all respiration-induced external torso motion captured, useful motion information can be extracted, including three useful breathing condition parameters: TV, TV′, and breathing pattern (BP). Four different breathing exercises were studied, including free breathing (FB), belly breathing (BB), chest breathing (CB), and breath hold (BH). These valuable pieces of information can join forces with the physical modeling approach[24] to produce a potentially accurate and reliable external tumor motion surrogate for clinical motion management in the future.

2. METHODS AND MATERIALS

Under an IRB-approved research protocol, eleven volunteers (five males and six females) with various body sizes (from small to extra large, based on leotard size measures) were recruited to participate in this study. Simultaneous measurements of the tidal volumes were performed using both an OSI system with three camera pods (AlignRT HD, Vision RT, London, UK) and a conventional spirometer (CPX, MedGraphics Corp., St. Paul, MN) as the standard for TV measurement. The two systems were synchronized before experiments using a standard time protocol (NISTimer, National Institute of Standard Technology, Gaithersburg, MD). A static OSI image was captured to establish an on-site reference surface image, while the high-speed image capture (HSIC) mode was applied to acquire images at 5 Hz. Detailed experimental conditions can be found below and elsewhere.[16]

2.A. Experimental characterization of OSI-based spirometry

Four types of breathing exercises were performed by the 11 participating volunteers in the following order: free, belly and chest breathing, breath hold, and then a repeated free breathing; each lasted at least 3 min with possible repetition. Subjects lay on a tilted (7.5°–10°) breast board (CIVCO, Coralville, IA), arms up in a supine position, and breathed through a preVent™ Pneumotach of a CPX spirometer. The torso surfaces, either the skin (male) or the skin covered by a form-fitting, light-colored leotard (female), were imaged using OSI. Volunteers were instructed to breathe using the belly in BB and the chest in CB. To demonstrate volume conservation within the torso and possibly different internal organ positions at any given TV, volunteers were asked to move the belly and chest up and down alternately during breath hold, mimicking the breathing motion. Two free breathing sessions were acquired at the beginning and end of the experiment to quantify breathing variations (or irregularities).

For each volunteer, at least two sessions of FB exercises were examined with an average total of 75 breathing cycles, ranging from 36 to 134 cycles. In addition to volume conservation, it was approximated that respiration-induced motion only involved the anterior surface as a subject lying in the supine position.[28,29] Previous studies based on 4DCT (Refs. 14 and 15) and OSI (Ref. 16) have validated these two assumptions. Therefore, the torso volume change measured by OSI represents the exchanging air volume in FB. We also assumed that negligible pressure variations can apply to BB, CB, and BH; this was tested under these breathing conditions.

2.B. Breathing pattern detected from OSI-based technique

Since OSI captured the motion of the entire torso, it is capable of allocating tidal volume distribution between the belly and chest. The superior boundary was near the clavicle and the inferior boundary was near the pubis, while the cut planes to separate the chest from belly were along the inferior edges of the ribcage. The BP measured by OSI was defined as the ratio of the volume changes in the chest (ΔV_{chest}) to the entire torso (ΔV_{torso}), namely,

$$\text{BP}^{\text{OSI}} = \frac{\Delta V_{\text{chest}}}{\Delta V_{\text{torso}}} = \frac{\Delta V_{\text{chest}}}{\text{TV}}. \quad (1)$$

BP^{OSI} quantifies the amount of intercostals involved, while diaphragm involvement is $1 - \text{BP}^{\text{OSI}}$ since $\text{TV} = \Delta V_{\text{torso}} = \Delta V_{\text{chest}} + \Delta V_{\text{belly}}$.

To link the volumetric BP^{OSI} to conventional chest/belly elevation during respiration as observed by surface fiducials, such as RPM, BP could be expressed as the ratio of the mean surface height variation of the chest to the torso. Surface height index (SHI) was next introduced,

$$\text{SHI}_{\text{ROI}} = \frac{1}{M \cdot N} \cdot \sum_{i,k=0}^{M,N} \Delta y(x_i, z_k), \quad (2)$$

where $\Delta y(x_i, z_k)$ is the anterior–posterior (AP) motion at a grid (x_i, z_k) within a 2D region of interest (ROI) in the *XOZ* Cartesian plane in reference to full-exhalation, and M and N are the total number of grids in the x and z directions, respectively. Then, BP^{SHI} can be defined as the ratio of chest height variation ($\text{SHI}_{\text{chest}}$) to the sum of chest and belly height variations ($\text{SHI}_{\text{chest}} + \text{SHI}_{\text{belly}}$), namely,

$$\text{BP}^{\text{SHI}} = \frac{\text{SHI}_{\text{chest}}}{\text{SHI}_{\text{chest}} + \text{SHI}_{\text{belly}}}. \quad (3)$$

By definition, the volume change within a ROI can be expressed as

$$\Delta V_{\text{ROI}} = \text{SHI}_{\text{ROI}} \cdot A_{\text{ROI}}, \quad (4)$$

where A_{ROI} is the area of the ROI projected to the *XOZ* plane. Therefore, BP^{SHI} describes the breathing pattern in height with a range (0, 1), similar to BP^{OSI}. In fact, when $A_{\text{chest}} \approx A_{\text{belly}}$ within the ROI, $\text{BP}^{\text{SHI}} \approx \text{BP}^{\text{OSI}}$. BP^{SHI} is useful for visualizing BP and torso respiratory motion.

2.C. Computation of torso volume change from OSI images

An in-house MATLAB computing program[30,31] was developed to perform automatic volume calculation with a user-defined volume of interest (VOI). The VOI is the anatomy volume inside the smallest geometric "box" defined by all 2D ROI constraints in two orthogonal (coronal and sagittal) views. It is worthwhile to note that the 3D geometric box (defines VOI) is fixed in the room coordinate system relative to the initial patient position. In posterior, superior, and inferior directions, the box defines VOI borders; whereas in anterior and lateral directions, torso surface defines the VOI. Typically, the box confines the same anatomy (the torso surface) of a subject, unless the subject moves his/her body relative to the initial position. The VOI was used for all OSI images during a breathing exercise, unless a baseline drift was observed due to a body position shift. Compared with the previous report,[16] we introduced a polygon, replacing the rectangular box, to define the ROI in the frontal view, as shown in Fig. 1. The user-defined ROI can include maximal moving torso surface while removing irrelevant regions and noises.

The VOI was defined in two orthogonal views. In the frontal view, a 2D ROI was defined by a user-drawn polygon (P) around left–right (LR) and superior–inferior (SI) borders. In the sagittal view, a tilted posterior coronal cut plane (C) around the body midline was determined. Two cut planes (T) along the inferior rib edges were used to separate the thorax and abdomen.

After the VOI was defined, a 3D Cartesian gridding (1×1 mm^2) and interpolation process were performed to reformat the Delaunay triangulation surface to a Cartesian 3D space: The grids on the *XOZ* plane (X = LR and Z = SI) enclosed all triangular nodes within the VOI, while the Y coordinate of every grid point (x, z) was computed by cubic interpolation of the adjacent Y coordinate (Y = AP) in the Delaunay triangular points. A Laplacian growing-based inpainting approach[32] was carried out to fill in the missing patches using the following partial differential equation (PDE):

$$I_t = \nabla^{\perp} I \cdot \nabla(\nabla \cdot \nabla I), \quad (5)$$

where I_t is the time derivative of the 3D surface image, $\nabla^{\perp}$ is the direction perpendicular to the gradient ∇I and the symbol $\cdot$ is the scalar product operator. Since the fixed point of this evolving PDE is $I_t = 0$, the inner product on the right-hand side of Eq. (5) translated to the desired effects of preserving the level lines, or isophytes, existing in the original image. The surface after this inpainting procedure is demonstrated in Figs. 1(B)–1(D).

The 3D surface image is converted into a 2D grid format. The grid (1×1 mm^2) is defined in a horizontal plane ($H = XOZ$) and a grid is a pixel of the surface. The grid column is defined by the grid projection (Y) perpendicular to the horizontal plane between the anterior surface (S) and posterior cut plane (C), or $h_s - h_c$. Here, we used the grid column as the element of VOI, and calculated the VOI volume by summing up the grid column volumes. For those unit squares sitting across the boundary of H, the corresponding volume was approximated by $(h_s - h_c) \times a$, a (<1) was the area of this bordering unit square inside H. Volumes for thoracic and abdominal regions were available based on separating planes S, as illustrated in Figs. 1(D) and 1(E). This algorithm was implemented in MATLAB to automatically compute the VOI volumes and torso volume changes as the tidal volumes.

2.D. Conventional spirometry measurement

Spirometric measurement was performed using a Bernoulli-type CPX spirometer with a preVent™ pressure sensor. The data acquisition was controlled by an in-house MATLAB program: the original 100 Hz sampling rate was reduced by averaging to 5 Hz to match the OSI acquisition speed. The

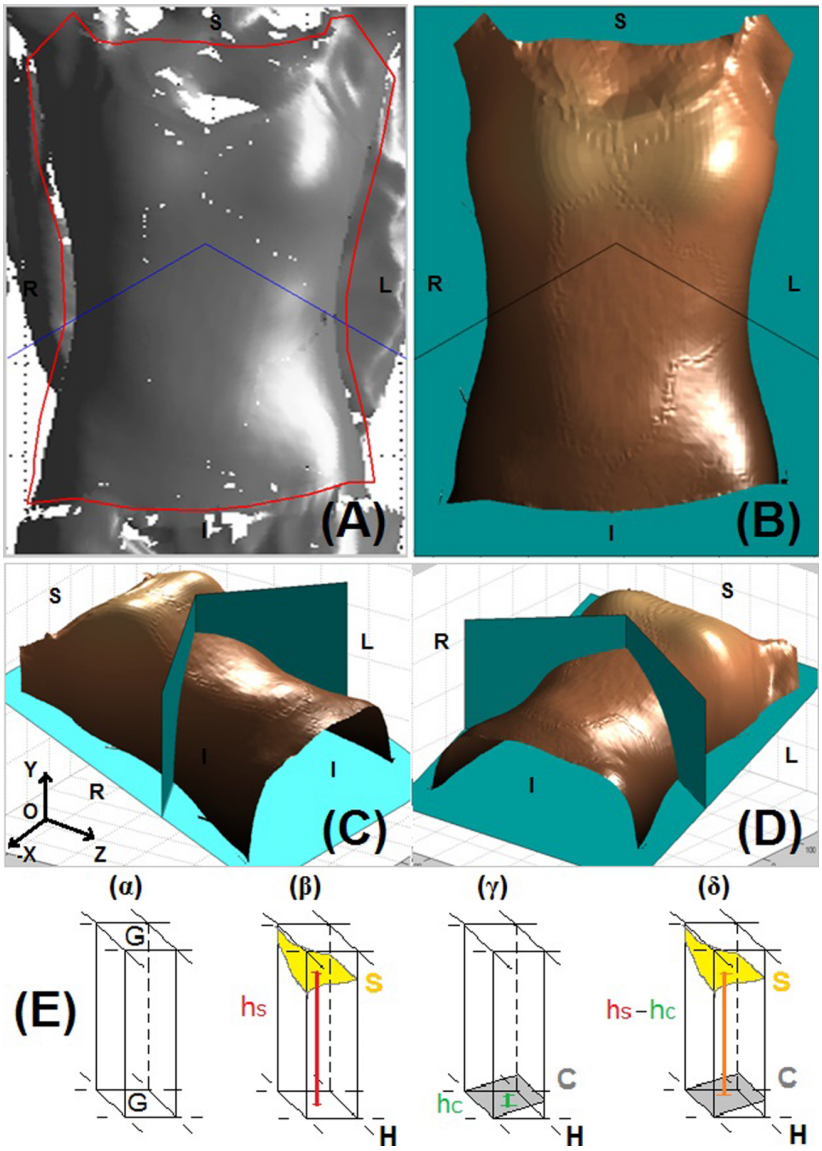

FIG. 1. Generation of a VOI and volume calculation. (A) a user-defined polygon (P, red) as the ROI to cover the torso and the separation cut plane (S) of the thorax and abdomen (blue) along the rib cage in the frontal view, (B) the processed 3D surface without "holes," (C) and (D) posterior tilted coronal cut plane (C, blue) around the midplane, and (E) the volumetric grid within the VOI and the parameters for volume calculation, in which G is the grid (1×1 mm^3), $H = XOZ$, C = coronal cut plane with a tilt as the torso is tilted (7.5°–10°), and S = body surface. The actual grid column, the element of the VOI, is between S and C and its volume = $(h_s - h_c)\times$area. The volume of VOI is the sum of all grid column volumes.

volume change ΔV during a time interval Δt was determined by the following equation,[30]

$$\Delta V = aR^{(b+1)}\Delta t, \tag{6}$$

where a and b were parameters determined by the calibration using a 3-l air syringe. Detailed procedure can be found in the previous publication.[16,33]

In order to compare the CPX-measured external TV (air volume measured outside the body) with the OSI-measured internal TV (due to internal volume change), a volumetric correction was performed using the ideal gas law to account for differences in temperature and partial water pressure inside the body and in the room. The correction factor of 1.08 (Ref. 34) was applied for inhalation volume only because inhaling air is at room condition when passing through the Pneumotach, while exhalation was left intact. The baseline shift due to this asymmetric operation was corrected based on a linear regression fit of the full-exhalation points as part of the offline data processing.

2.E. Data processing and analysis

After the experiments, the 4–5 Hz HSIC raw data (2 GB/min) were retrospectively extracted to reconstruct a series of 3D OSI surface images in batch mode using the RawDataExtraction program (VisionRT, London, UK). Based on these surface images, a VOI was defined and the volume within the VOI was calculated. For each breathing exercise, one VOI was defined and used for the entire image series for tidal volume calculation. The accuracy of OSI-based spirometry, in reference to the conventional spirometry, was assessed in static (peak-to-valley) and/or dynamic (point-by-point) formats. The

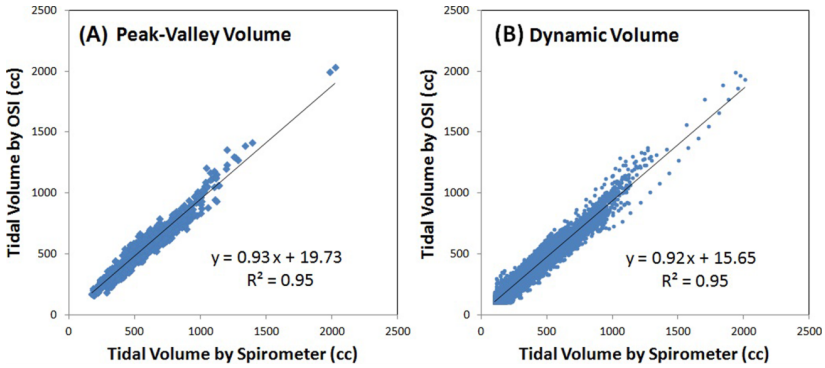

FIG. 2. Linear regression fittings ($R^2 = 0.95$) of tidal volume range [(A), peak-to-valley, 837 breathing cycles, slope = 0.93] and dynamic tidal volume [(B), point-by-point, 42 615 measured points, slope = 0.92] between the OSI and CPX measurements. (Data with TV < 100 cm^3 are ignored.)

OSI-based airflow was calculated by taking the first-order time derivative of the TV values after a five-point moving average was performed; while CPX-based airflow was calculated, the data was down-sampled from 100 to 5 Hz. The quantity BP was evaluated from the OSI data only and visualized using color-coded SHI representation. The different motions between different breathing patterns were visualized and compared. For two free breathing exercises, the reproducibility was assessed based on TV, BP, and the breathing period.

Unlike conventional spirometry, the OSI-based spirometry was generally free from the baseline drift.[9,16] However, a baseline drift may occur if a subject's body moves during the experiment, because the user-defined geometric ROI box is fixed in space and the actual VOI could be changed if the subject body moved. The body shift can be identified by surface image registration and therefore corrected with AlignRT guidance.

3. RESULTS

3.A. Tidal volume measurement and accuracy

The linear regression fittings between OSI and CPX measurements are depicted in Fig. 2. Both peak-valley and dynamic volume comparisons depict that the OSI measured TV is similar within 5%. However, OSI values are consistently smaller than CPX-measured values in most measurements.

The accuracy of the maximal tidal volume (peak-to-valley) of the OSI measurement using CPX as the standard is reported in Table I. The mean difference among all subjects is -21 ± 27 cm^3 (ranging from 26 to -68 cm^3) or $-3.5\% \pm 6.3\%$ (ranging from -9.8% to 5.4%). These values are consistent with the linear regression analysis, suggesting that OSI slightly underestimates the TV value. Further lowering the posterior cut plane from the midline in VOI definition may improve the TV value by about 1%. The mean measured TV is 512 ± 147 cm^3 by OSI and 533 ± 157 cm^3 by the CPX spirometer.

3.B. Air flow rate in subject respiration

The airflow data can be obtained by calculating the first time derivative of the TV curve, as tabulated in Table II. Some random noises were removed by averaging the CPX spirometric data from 100 to 5 Hz. To match the data quality, a five-point moving average was applied to the OSI data. Airflow

TABLE I. Accuracy of OSI-based spirometry in TV measurement.

		Tidal volume (cm^3)							
		Spirometer		OSI		Error (cm^3)		Relative error (%)	
Human subject	Number of breaths	Average	Standard deviation	Average	Standard deviation	Average	Standard deviation	Average	Standard deviation
1	134	600	117	581	104	−19	34	−2.7	6.0
2	111	361	72	367	62	6	24	2.5	6.8
3	90	498	109	524	117	26	44	5.4	9.2
4	74	713	226	645	213	−68	45	−9.2	5.6
5	69	489	78	476	75	−12	23	−2.4	4.8
6	85	325	65	322	60	−3	28	−0.4	8.7
7	59	865	173	849	202	−16	47	−2.4	5.4
8	59	545	159	501	164	−44	36	−8.8	7.6
9	36	565	139	512	124	−53	29	−9.4	3.9
10	58	384	75	364	78	−20	26	−5.1	7.1
11	62	521	66	489	68	−32	23	−6.2	4.5
Average	76	533	116	512	115	−21	33	−3.5	6.3
Standard deviation	28	157	53	147	56	27	9	4.8	1.7

TABLE II. Comparison of TV′ measured by conventional and OSI-based spirometers. The mean airflows in inhalation and exhalation (peak-valley) and the dynamic airflow (point-by-point) are provided.

	Mean airflow (peak and valley)						Dynamic airflow Airflow difference	
	Spirometer airflow			OSI airflow				
Human subjects	Overall (cm^3/s)	Inhale (cm^3/s)	Exhale (cm^3/s)	Overall (cm^3/s)	Inhale (cm^3/s)	Exhale (cm^3/s)	Mean Δ (cm^3/s)	Standard deviation (cm^3/s)
1	281	329	256	267	351	222	−0.4	60.9
2	211	267	180	215	258	187	−0.2	43.8
3	230	250	218	240	268	220	−0.5	52.0
4	336	397	304	301	357	268	−1.0	69.1
5	190	266	150	186	261	146	−0.9	44.0
6	259	254	272	251	264	242	−1.0	50.6
7	481	526	446	468	527	425	−2.0	67.4
8	421	473	386	388	449	345	−0.6	71.6
9	253	287	233	236	268	213	−0.4	46.5
10	214	251	189	205	246	178	−0.6	41.4
11	255	263	257	243	276	220	−0.6	45.0
Average	285	324	263	273	320	242	−0.8	53.9
Standard deviation	92	98	89	85	92	80	0.5	11.3

in inhalation is greater than that in exhalation during FB in most cases. The mean difference between these two sets of data is small (−0.8 cm^3/s, Table II) among all subjects. However, the standard deviation for each subject is large (54 cm^3/s), as the first derivative is sensitive to the random noises in the data.

3.C. OSI-measured tidal volumes in three breathing patterns

A plot of TV(OSI) versus TV(CPX) for all subjects in FB, BB, and CB is shown in Fig. 3. The slopes (with correlation) of the regression lines are: 0.93 (0.98) for FB, 0.96 (0.99) for BB, and 0.95 (0.98) for CB. These values suggest that OSI-based spirometry produces accurate TV measurement under these three conditions. The peak-to-valley TV of these breathing exercises vary from <500 to >2000 cm^3 among the participating individuals.

Table III tabulates the BP and TV values from the three breathing exercises. BP values indicate a steady trend, consistently increasing from BB to FB and CB (Fig. 5). The TV values of BB and CB may vary depending on individual behaviors (Fig. 6) but are persistently greater than those in FB. The visual SHI difference (ROI = the torso) between the three breathing patterns is illustrated in Fig. 4.

3.D. Quantifying breathing irregularities with TV and BP

Changing breathing mode from one to another is a special type of breathing irregularity, reflected by not only TV but also BP (Figs. 5 and 6). Table IV demonstrates irreproducible breathing irregularities between separate acquisitions with a time interval of 29 ± 9 min in terms of tidal volume (amplitude), period (or frequency), and breathing pattern (thorax vs abdomen). These three parameters vary substantially with the ranges of: (−64%, 40%) for tidal volume, (−50%, 26%) for period, and (−49%, 44%) for breathing pattern. Table V reports the breathing irregularities in airflow; within the same exercise, airflow is greater in inhalation than in exhalation during normal free breathing.

3.E. Different organ motions at a given tidal volume

Table VI depicts that on average, 4% TV fluctuations occurred when subjects moved the belly and chest up and down alternately during BH, suggesting that volume is conserved when there is no air exchange. Table VI also showed a large BP variation (0–1) during the BH exercise, indicating that respiration-induced organ motion could be predominant in SI or AP directions based on BP value.

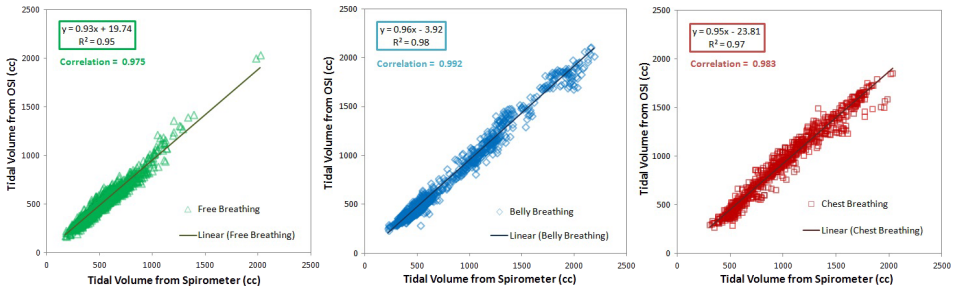

FIG. 3. Linear regression and correlation between OSI- and CPX-spirometric measurements of TV (peak-to-valley) in FB, BB, and CB.

TABLE III. Breathing pattern [BP^{OSI}, defined in Eq. (1)] and TV in three breathing exercises. The BP increasing order is BB, FB, and CB, while the TV increasing order is FB, BB, and CB.

	Free breathing		Belly breathing		Chest breathing	
Volunteer	BP[a]	OSI TV (cm^3)	BP	OSI TV (cm^3)	BP	OSI TV (cm^3)
1	0.11	581	0.05	1743	0.56	1366
2	0.49	367	0.20	402	0.94	465
3	0.23	524	—	427	0.61	973
4	0.32	645	0.15	706	0.55	1530
5	0.16	476	0.04	1297	0.72	1064
6	0.36	322	0.11	424	0.87	480
7	0.13	849	—	1057	0.39	881
8	0.44	501	0.26	1042	0.75	848
9	0.29	512	0.08	1081	0.99	1173
10	0.37	364	0.16	577	0.68	1159
11	0.32	489	0.19	491	0.61	664
Average	0.29	512	0.14	841	0.70	964

[a]Two BP^{OSI} values are not reported since the volunteers were incapable of belly breathing.

4. DISCUSSION

4.A. Sources of uncertainty in tidal volume measurement using OSI

The completion of torso coverage in the VOI is the most important factor in the OSI-based spirometry. Table I signifies that the OSI underestimates the TV by −3.5% on average. Using the ceiling-mounted AlignRT camera system, the moving torso surface, namely, the entire anterior and most lateral torso surface, is visible in the field of view, as shown in Fig. 1. The static surface in the posterior side does not contribute to the volume change; therefore, this constant term will be canceled out when calculating torso volume change. In this study, we demonstrate that OSI-based spirometry can be applied to measure TV accurately in various breathing conditions (FB, BB, and CB), as shown in Table III and Fig. 6. In the BH experiment, a near constant TV verifies the volume conservation (Fig. 7).

A user-defined polygon includes the FOV in the frontal view: the superior boundary was near the clavicle and the inferior boundary was near the pubis. If the inferior border is covered by a gown or blanket, it may underestimate the tidal volume [Fig. 1(A)], as most people are belly-dominant (BP < 0.5) breathers[14] (Table III). When applying the posterior cut plane at the sagittal midline, there is a known 0.3%–1.2% shortage of tidal volume. In other words, the overall accuracy could be improved by about 1% if the posterior cut plane is lowered by 1–2 cm. Further lowering the cut plane could introduce another type of uncertainty because of a bi-value function problem in surface image processing, namely two surface points could be found for a given (x, z) point in the grid near the lateral edge. In this case, the program may introduce a large artificial uncertainty when processing the surface and thus affects the volume calculation. This error can be visualized as the body edge is altered and avoided by raising the cut plane slightly.

The OSI surface images contain holes, which need to be patched by the PDE-based inpainting process in the initial processing (Fig. 1). When the holes are located in a featured landscape, such as the upper chest area, respiratory motion makes the size, shape, and position of the holes irreproducible. Therefore, small random noises are introduced, which affect the calculation accuracy of the tidal volume as well as airflow (Fig. 5).

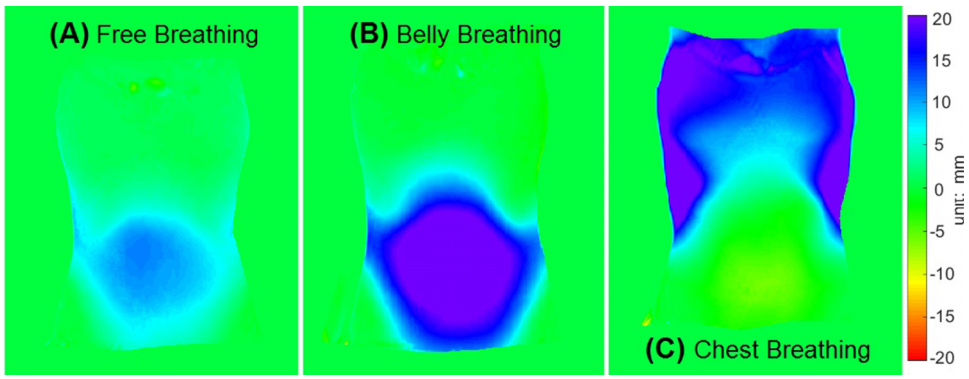

FIG. 4. Visual representation [SHI_{torso}, defined in Eq. (2) with ROI = torso] of four subjects' respiratory motions in three breathing modes: (A) free breathing (BP = 0.22, TV = 512 cm^3), (B) belly breathing (BP = 0.04, TV = 1081 cm^3), and (C) chest breathing (BP = 0.98, TV = 1173 cm^3). The BB and CB are two extremes: using primarily the diaphragm and intercostals, respectively; while FB is often mixed with BB and CB.

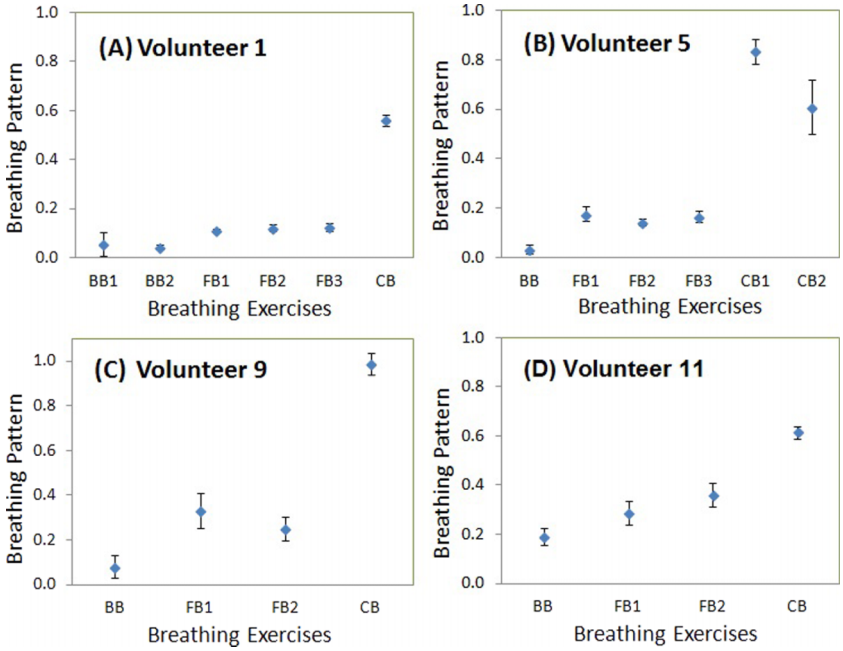

FIG. 5. Four examples of breathing pattern variations among three breathing exercises. By definition, BP value is the lowest for BB and the highest for CB. The BP value in FB is more like those in BB for most volunteers.

On the other hand, uncertainty in conventional spirometry also affects the accuracy evaluation of the OSI-based spirometry. It is well-known that conventional spirometry carries an uncertainty of ±3%.[35] The Bernoulli-type spirometer was the best available spirometer, which was previously developed and characterized to measure dynamic tidal volume.[33] In this study, we observed ±3% uncertainty during a test after calibrations and a further correction was applied. In addition, the calibration is performed at five typical airflow rates that correspond to those for normal free breathing (Table IV). While the normal calibration may not work at a very high flow rate, such an extremely high airflow was not observed in free breathing.

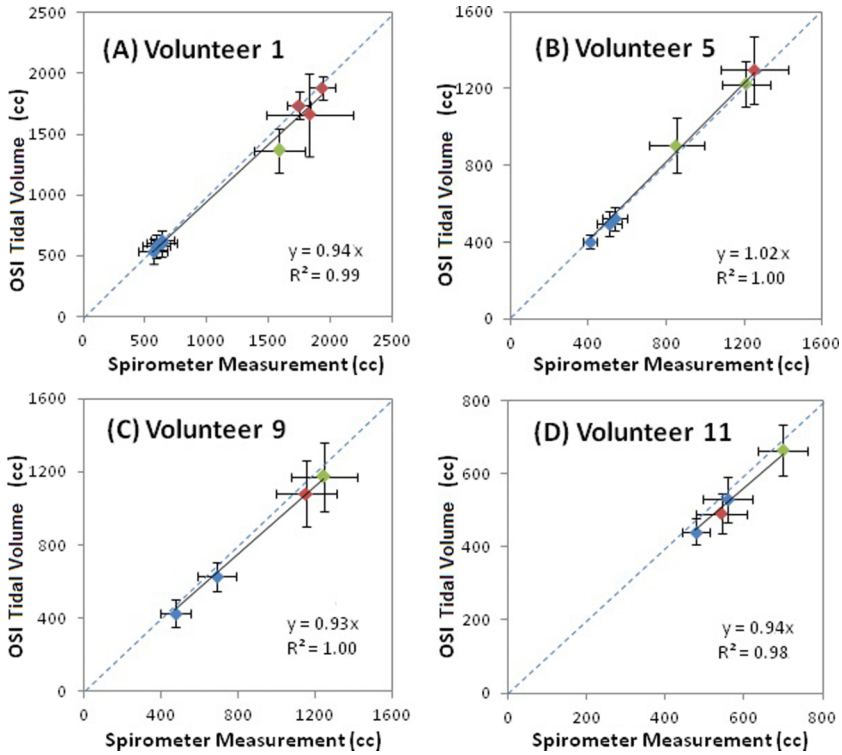

FIG. 6. Linear regression fitting (interception disabled) between the OSI- and CPX-spirometric measurements of tidal volume (peak-to-valley) in free breathing (blue), belly breathing (red), and chest breathing (green) in four volunteers. The two orthogonal, similar-in-length error bars (1σ) represent breathing irregularities measured by the two techniques.

TABLE IV. Breathing irregularities (irreproducibility in two free breathing sessions) in TV, period, and BP measured by the OSI technique in about 30-min time intervals. (Δ/mean = difference/mean of the two values).

			Tidal volume (cm^3)			Period (s)		Breathing pattern		
Human subject	Number of breaths	Time interval (min)	Mean	Standard deviation	Δ/mean (%)	Mean	Δ/mean (%)	Mean	Standard deviation	Δ/mean (%)
1	26	35	601	111	10.3	4.6	2.0	0.12	0.02	35.9
	48		542	102		4.5		0.09	0.02	
2	42	52	375	40	−7.8	3.8	12.2	0.44	0.04	−48.6
	35		405	56		3.3		0.72	0.21	
3	28	33	432	59	−42.8	3.5	−50.1	0.20	0.03	−21.3
	15		667	59		5.9		0.25	0.04	
4	24	29	740	106	40.3	4.4	25.7	0.33	0.03	14.9
	25		492	88		3.4		0.28	0.03	
5	25	35	522	62	25.9	5.4	6.4	0.18	0.03	5.4
	21		403	33		5.0		0.17	0.02	
6	36	23	353	39	16.3	2.9	20.3	0.31	0.04	25.3
	49		300	62		2.4		0.39	0.11	
7	23	23	709	85	−27.8	3.6	2.9	0.16	0.03	32.0
	36		939	205		3.5		0.11	0.04	
8	22	22	314	63	−64.3	2.9	14.9	0.31	0.04	−49.1
	37		612	84		2.5		0.52	0.07	
9	15	21	627	78	37.5	4.4	14.9	0.33	0.08	27.1
	21		429	75		3.8		0.25	0.05	
10	32	24	332	49	−20.0	3.3	1.7	0.44	0.08	44.4
	26		405	88		3.3		0.28	0.11	
11	33	22	530	63	18.1	3.8	−3.6	0.29	0.05	−22.8
	29		442	35		3.9		0.36	0.05	
Average		29			−1		4			−1
Standard deviation		9			34		20			34
Range					−64, 40		−50, 26			−49, 44

Baseline drift is well-known for conventional spirometry; the correction scheme is based on the assumption that five consecutive breaths have reproducible full exhalations. However, occasional outliers in the full-exhalation stage were detected and a retrospective baseline correction was performed to eliminate these outliers and regroup the five consecutive cycles for correction.

4.B. BP: The spatial distribution of OSI-measured TV

It is clear that OSI can view the entire torso, and thus covering all respiratory-induced external body motion (Fig. 1). Therefore, torso surface motion provides real-time boundary conditions of respiratory motion and, in principle, this information can be utilized to unveil the motion of internal organs with the assistance of biomechanical modeling.[21,36] Although partial body surface is observed, only the moving surface matters; whereas stable surface remains unchanged, and can be obtained by fusion with simulation CT as necessary. This is an approach that could overcome the fundamental limitation of a correlation-based internal–external relationship in organ motion prediction.

Breathing pattern is a spatial parameter to quantify the TV distribution within the torso cavities, as illustrated in Fig. 4. This is a unique feature of the OSI-based technique to quantify a spatial feature of the torso motion, while conventional spirometry can only produce TV, a scale parameter, lack of spatial direction and distribution. Previous studies indicated that conceptually separating the orthogonal AP and SI motion in the lung, BP^{lung} can be extracted from 4DCT to predict AP and SI motions of the mean diaphragm position.[14,15] It has also been widely reported that the correlation between diaphragmatic and tumor motion is usually high, such as 0.94–0.98;[37,38] thus this BP approach could be extended to further predict tumor motion.

4.C. Advantages of OSI-based spirometry

The purpose of this new OSI-based spirometry is to produce three real-time respiratory parameters (TV, TV′, and BP), together with possible body shifts, which are useful to feed a physical perturbation model for tumor motion prediction.[14–16,25] To this end, the advantages of the OSI-based spirometry can be summarized in the following three aspects: (1) accurate tidal volume and airflow measurements, (2) breathing pattern quantification as a new breathing descriptor, and (3) the detection and correction of body shift by surface image registration.

Non-invasive, OSI-based spirometry eliminates patient inconvenience or difficulties when breathing through a tube with their nose clamped. During this volunteer study, a break time every 5–10 min was needed to allow subjects to take

TABLE V. Breathing irregularities in airflow (overall, inhalation, and exhalation) measured by the OSI technique in about 30-min time intervals. (Δ/mean = difference/mean of two replicates).

		Overall		Inhalation		Exhalation	
Human subject	Time interval (min)	Average (cm^3/s)	Δ/mean (%)	Average (cm^3/s)	Δ/mean (%)	Average (cm^3/s)	Δ/mean (%)
1	35	270	7.5	364	10.5	221	5.7
		250		328		209	
2	52	202	−19.2	252	−13.4	171	−23.4
		245		288		216	
3	33	242	6.4	270	12.9	220	0.6
		227		237		219	
4	29	344	18.4	420	31.3	295	8.0
		286		306		272	
5	35	196	20.2	272	24.4	155	17.7
		160		213		130	
6	23	244	−5.2	257	−4.8	234	−5.7
		257		270		248	
7	23	392	−29.2	446	−26.0	352	−31.8
		526		579		485	
8	22	217	−77.2	278	−65.6	177	−86.2
		490		550		445	
9	21	284	23.2	341	31.0	247	17.9
		225		249		207	
10	24	200	−21.4	246	−20.4	170	−22.3
		248		302		212	
11	22	281	21.7	349	41.1	236	5.5
		226		230		223	
Average	29		−5		2		−10
Standard deviation	9		30		32		30
Range			−77, 23		−66, 41		−86, 18

off the mouthpiece and nose clamp. Further increasing OSI performance in data acquisition and processing could improve the accuracy of the TV and TV′ measurement. OSI-based spirometry also detects breathing pattern and body shift, which are unique features beyond conventional spirometry. BP is one of the simplest means to utilize the TV distribution within the torso surface; other more sophisticated methods could be developed. As an imaging tool, the voluntary body shift can also be identified and corrected through surface image registration. Graduate body shift can result in tumor motion baseline drift,[39] which affects treatment accuracy. The OSI-based technique, in principle, can effectively detect, quantify, and serve as a guide to correct the body shift. Therefore, the OSI-based technique should be further fully exploited

TABLE VI. Volume conservation during the BH exercise. The large BP variation with a small fluctuation in TV indicates volume conservation with a small uncertainty.

			TV (cm^3) at BH		Fluctuation (standard deviation/mean) (%)	BP^{OSI}[a]	
Volunteer	Gender	Size	Mean	Standard deviation		Min	Max
1	M	XL	1134	79	7	0.01	0.86
2	F	M	533	25	5	0.13	1.38
3	F	XL	802	34	4	0.51	1.16
4	M	L	1431	39	3	0.45	0.65
5	M	M	769	18	2	−0.10	0.67
6	F	L	1086	16	1	0.57	0.96
7	M	L	1204	54	5	−0.06	0.69
8	F	S	824	23	3	0.17	0.56
9	F	M	600	20	3	0.17	1.20
10	M	M	<300[b]	—	—	—	—
11	F	M	977	48	5	−0.05	0.63
Average					4	0.18	0.88

[a]The BP <0 or >1 is because the chest or belly surface moved under the reference full-exhalation image.
[b]No BH-TVs in this case is greater than 300 cm^3, resulting in large fluctuation and unreliable BP.

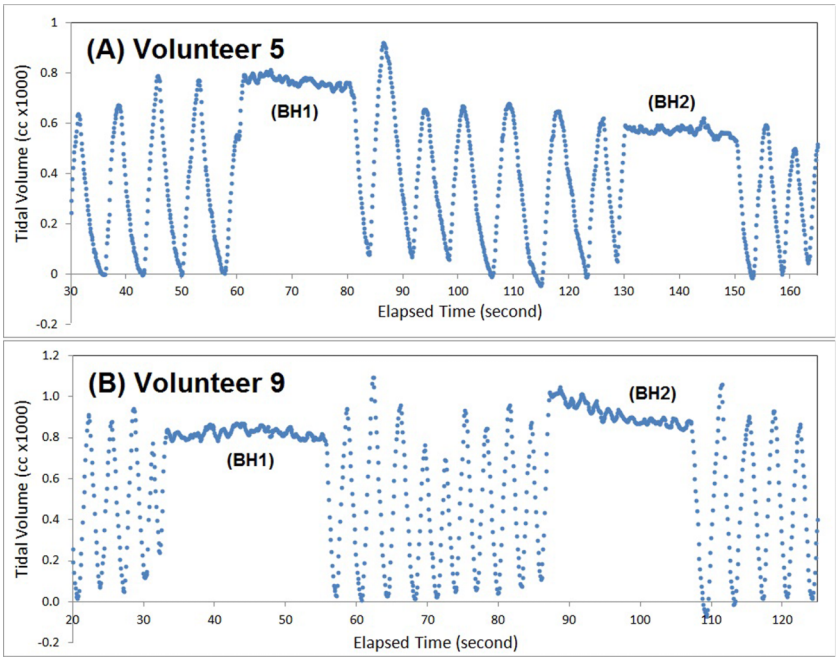

FIG. 7. Two examples of OSI-based spirometric data during breath-holding (BH) motion exercises, in which chest and belly moved up and down to mimic breathing motion. As there was no air exchange during the BH periods, a relatively constant TV with a minimal variation was observed in the OSI measurements. In (B), the BH2 the tidal volume drift is due to the subject's body shift when putting efforts into the motion exercise during BH.

in intrafractional motion monitoring for image-guided radiotherapy.

The three respiratory parameters (TV, TV′, and BP) could be used as real-time updates to a physical model for tumor motion prediction, which is promising as all external motions are captured by this OSI-based technique. Inclusion of multiple surface points[40] and larger surface ROIs (Ref. 10) for motion monitoring were studied, depicting an improved performance in correlation-based tumor motion prediction. As the ROI increases from local areas to the entire torso surface, it creates a pseudoclosed physical system, from which three pieces of motion information are concurrently available: (1) all respiratory-induced external motion, (2) TV and TV′ from torso volume change, and (3) BP based on TV distribution between the thorax and abdomen. They are potentially useful to predict tumor motion based on physics, rather than correlation that changes with patient respiratory behavior.[41] Previously, we have presented a physical perturbation model to account for breathing irregularities and to estimate internal diaphragm/tumor motion from external torso motion.[25] Further investigations could lead to a clinically implementable tool to predict tumor motion in the presence of breathing irregularities.

4.D. Limitation and future directions

The current OSI-based technique cannot provide real-time results yet, although HSIC mode can capture 5 Hz image rate at the highest surface image resolution. The raw data need to be retrospectively reconstructed to form a series of 3D surfaces. The field of view is extremely large, as shown in Fig. 1, and the reconstruction takes approximately 1 s per 3D surface image. For OSI image processing and volume calculation, it takes another second per image including image data loading. However, the current performance (2 s) is not far from real-time performance, especially with integration of different algorithms in one platform to avoid repeating image data saving/loading when processed in separated programs, and with enhancement from parallel computing based on graphics processing unit (GPU) and multiple cores/servers/clusters, which can often improve performance by 1–2 orders of magnitude.[42,43] The GPU technology has been applied in real-time volumetric image registration[42] and real-time tumor motion prediction using projection images during cone beam computed tomography (CBCT) scan.[44] Most importantly, it is necessary to gain collaborative support from the vendor in order to implement GPU technology, plug in the volume calculation, and add latency handling into the commercial software to facilitate real-time performance.

To address the issue of possible view blocking by the gantry and gantry-mounted kV and MV arms, it is necessary to change the current AlignRT configuration, which contains three ceiling-mounted camera pods on a patient's left, right, and inferior sides. To minimize the view blocking problem, one possible solution is to implement a four-camera system. A possible new configuration would have two front camera pods, instead of one currently, with ±20° from the couch zero position. Under this configuration, the isocenter can always be viewed throughout a 360° gantry rotation. We have simulated the OSI images at the suggested angles by rotating the couch ±20°–30° with a volunteer on the table. Therefore, this is a feasible solution, but again requires the vendor's efforts to support the implementation. Further investigations to overcome these limitations are needed for a successful clinical implementation of the OSI-based motion management technique.

5. CONCLUSION

We have established a new OSI-based motion monitoring technique that utilizes a physical relationship to measure tidal volume, airflow, and breathing pattern. The accuracy of the tidal volume by OSI measurement is $-3.5\% \pm 6.3\%$ on average, compared with conventional spirometry, while the mean discrepancy in airflow is -0.8 ± 54 cm^3/s. Accurate measurements can be performed in various breathing patterns, such as FB, BB, and CB. Spatial quantifications, such as detection of breathing pattern and body misalignment, are unique features of the OSI-based technique. Using the OSI-based technique, substantial breathing irregularities and irreproducibility were observed and quantified. These respiratory parameters are useful to monitor respiratory motion and motion variation caused by breathing irregularities, and can collaborate with a potential physical model to tackle the bottleneck in correlation-based external tumor motion surrogating.

ACKNOWLEDGMENTS

This work is supported in part by the National Institutes of Health (Nos. U54CA137788 and U54CA132378) and by the MSK Cancer Center Support Grant/Core Grant (No. P30 CA008748). The authors are grateful to Mr. Matthew O'Brien at University of Wisconsin for donating a conventional spirometer to this research project and thank Dr. Tiezhi Zhang and Dr. Bhudatt Paliwal (University of Wisconsin) for sharing their knowledge and experience on programming to control the spirometer. We are also grateful to VisionRT for their technical support on HSIC and RTD. The authors are grateful to Ms. Joan Zatchy, R.N. (MSK), for the assistance in the volunteer study, and Mr. James Sullivan (MSK) for his help and lending the 3L air syringe for spirometry calibration. The authors thank all the volunteers (G.D., L.F., E.A., K.S., M.S., N.A., M.C., A.K., J.V., K.C., N.V., and M.O.) who participated in this clinical research. The authors report no conflicts of interest in conducting the research.

[a]Author to whom correspondence should be addressed. Electronic mail: lig2@mskcc.org

[1]P. J. Keall, G. S. Mageras, J. M. Balter, R. S. Emery, K. M. Forster, S. B. Jiang, J. M. Kapatoes, D. A. Low, M. J. Murphy, B. R. Murray, C. R. Ramsey, M. B. van Herk, S. S. Vedam, J. W. Wong, and E. Yorke, "The management of respiratory motion in radiation oncology report of AAPM Task Group 76," Med. Phys. **33**, 3874–3900 (2006).

[2]J. W. Wolthaus, J. J. Sonke, M. van herk, and E. M. Damen, "Reconstruction of a time-averaged midposition CT scan for radiotherapy planning of lung cancer patients using deformable registration," Med. Phys. **35**, 3998–4011 (2008).

[3]J. R. Olsen, W. Lu, J. P. Hubenschmidt, M. M. Nystrom, P. Klahr, J. D. Bradley, D. A. Low, and P. J. Parikh, "Effect of novel amplitude/phase binning algorithm on commercial four-dimensional computed tomography quality," Int. J. Radiat. Oncol., Biol., Phys. **70**, 243–252 (2008).

[4]H. Li, C. Noel, J. Garcia-Ramirez, D. Low, J. Bradley, C. Robinson, S. Mutic, and P. Parikh, "Clinical evaluations of an amplitude-based binning algorithm for 4DCT reconstruction in radiation therapy," Med. Phys. **39**, 922–932 (2012).

[5]S. S. Korreman, T. Juhler-Nottrup, and A. L. Boyer, "Respiratory gated beam delivery cannot facilitate margin reduction, unless combined with respiratory correlated image guidance," Radiother. Oncol. **86**, 61–68 (2008).

[6]R. L. Smith, D. Yang, A. Lee, M. L. Mayse, D. A. Low, and P. J. Parikh, "The correlation of tissue motion within the lung: Implications on fiducial based treatments," Med. Phys. **38**, 5992–5997 (2011).

[7]H. Fayad, T. Pan, J. F. Clement, and D. Visvikis, "Technical note: Correlation of respiratory motion between external patient surface and internal anatomical landmarks," Med. Phys. **38**, 3157–3164 (2011).

[8]P. J. Schoffel, W. Harms, G. Sroka-Perez, W. Schlegel, and C. P. Karger, "Accuracy of a commercial optical 3D surface imaging system for realignment of patients for radiotherapy of the thorax," Phys. Med. Biol. **52**, 3949–3963 (2007).

[9]S. Hughes, J. McClelland, S. Tarte, D. Lawrence, S. Ahmad, D. Hawkes, and D. Landau, "Assessment of two novel ventilatory surrogates for use in the delivery of gated/tracked radiotherapy for non-small cell lung cancer," Radiother. Oncol. **91**, 336–341 (2009).

[10]C. K. Glide-Hurst, D. Ionascu, R. Berbeco, and D. Yan, "Coupling surface cameras with on-board fluoroscopy: A feasibility study," Med. Phys. **38**, 2937–2947 (2011).

[11]E. W. Pepin, H. Wu, Y. Zhang, and B. Lord, "Correlation and prediction uncertainties in the cyberknife synchrony respiratory tracking system," Med. Phys. **38**, 4036–4044 (2011).

[12]F. Ernst, R. Bruder, A. Schlaefer, and A. Schweikard, "Correlation between external and internal respiratory motion: A validation study," Int. J. Comput. Assisted Radiol. Surg. **6**, 93–101 (2011).

[13]K. Malinowski, T. J. McAvoy, R. George, S. Dieterich, and W. D. D'Souza, "Online monitoring and error detection of real-time tumor displacement prediction accuracy using control limits on respiratory surrogate statistics," Med. Phys. **39**, 2042–2048 (2012).

[14]G. Li, N. C. Arora, H. Xie, H. Ning, W. Lu, D. Low, D. Citrin, A. Kaushal, L. Zach, K. Camphausen, and R. W. Miller, "Quantitative prediction of respiratory tidal volume based on the external torso volume change: A potential volumetric surrogate," Phys. Med. Biol. **54**, 1963–1978 (2009).

[15]G. Li, H. Xie, H. Ning, W. Lu, D. Low, D. Citrin, A. Kaushal, L. Zach, K. Camphausen, and R. W. Miller, "A novel analytical approach to the prediction of respiratory diaphragm motion based on external torso volume change," Phys. Med. Biol. **54**, 4113–4130 (2009).

[16]G. Li, H. Huang, J. Wei, D. G. Li, Q. Chen, C. P. Gaebler, J. Sullivan, J. Zatcky, A. Rimner, and J. Mechalakos, "Novel spirometry based on optical surface imaging," Med. Phys. **42**, 1690–1697 (2015).

[17]C. Ozhasoglu, C. B. Saw, H. Chen, S. Burton, K. Komanduri, N. J. Yue, S. M. Huq, and D. E. Heron, "Synchrony–cyberknife respiratory compensation technology," Med. Dosim. **33**, 117–123 (2008).

[18]D. A. Low, P. J. Parikh, W. Lu, J. F. Dempsey, S. H. Wahab, J. P. Hubenschmidt, M. M. Nystrom, M. Handoko, and J. D. Bradley, "Novel breathing motion model for radiotherapy," Int. J. Radiat. Oncol., Biol., Phys. **63**, 921–929 (2005).

[19]T. Zhao, W. Lu, D. Yang, S. Mutic, C. E. Noel, P. J. Parikh, J. D. Bradley, and D. A. Low, "Characterization of free breathing patterns with 5D lung motion model," Med. Phys. **36**, 5183–5189 (2009).

[20]T. Zhao, B. White, K. L. Moore, J. Lamb, D. Yang, W. Lu, S. Mutic, and D. A. Low, "Biomechanical interpretation of a free-breathing lung motion model," Phys. Med. Biol. **56**, 7523–7540 (2011).

[21]A. Al-Mayah, J. Moseley, M. Velec, and K. K. Brock, "Sliding characteristic and material compressibility of human lung: Parametric study and verification," Med. Phys. **36**, 4625–4633 (2009).

[22]R. Werner, J. Ehrhardt, R. Schmidt, and H. Handels, "Patient-specific finite element modeling of respiratory lung motion using 4D CT image data," Med. Phys. **36**, 1500–1511 (2009).

[23]M. Li, E. Castillo, X. L. Zheng, H. Y. Luo, R. Castillo, Y. Wu, and T. Guerrero, "Modeling lung deformation: A combined deformable image registration method with spatially varying Young's modulus estimates," Med. Phys. **40**, 081902 (10pp.) (2013).

[24]J. Eom, X. G. Xu, S. De, and C. Shi, "Predictive modeling of lung motion over the entire respiratory cycle using measured pressure-volume data, 4DCT images, and finite-element analysis," Med. Phys. **37**, 4389–4400 (2010).

[25]G. Li, A. Yuan, and J. Wei, "An analytical respiratory perturbation model for lung motion prediction," Med. Phys. **41**, 473 (2014).

[26]G. Li, A. Ballangrud, L. C. Kuo, H. Kang, A. Kirov, M. Lovelock, Y. Yamada, J. Mechalakos, and H. Amols, "Motion monitoring for cranial frameless stereotactic radiosurgery using video-based three-dimensional optical surface imaging," Med. Phys. **38**, 3981–3994 (2011).

[27]C. Bert, K. G. Metheany, K. Doppke, and G. T. Chen, "A phantom evaluation of a stereo-vision surface imaging system for radiotherapy patient setup," Med. Phys. **32**, 2753–2762 (2005).
[28]G. Li, H. Xie, H. Ning, N. Arora, A. Brown, P. Guion, J. Cheng, B. Arora, A. Kaushal, D. Citrin, K. Camphausen, and R. W. Miller, "A feasibility study of image registration using volumetrically classified, motion-free bony landmarks in thoracic 4DCT images for image-guided patient setup," Int. J. Biomed. Eng. Technol. **8**, 259–273 (2012).
[29]G. Li, P. Cohen, H. Xie, D. Low, D. Li, and A. Rimner, "A novel four-dimensional radiotherapy planning strategy from a tumor-tracking beam's eye view," Phys. Med. Biol. **57**, 7579–7598 (2012).
[30]J. Wei, A. Yuan, and G. Li, "An automatic toolkit for efficient and robust analysis of 4D respiratory motion (BEST IN PHYSICS)," Med. Phys. **41**, 473 (2014).
[31]J. Wei and G. Li, "Automated lung segmentation and image quality assessment for clinical 3D/4D computed tomography," IEEE J. Transl. Eng. Health Med. **2**, 1800110 (10pp.) (2014).
[32]J. Wei, "Lesbesgue anisotropic image denoising," Int. J. Imaging Syst. Technol. **15**, 64–72 (2005).
[33]T. Zhang, H. Keller, M. J. O'Brien, T. R. Mackie, and B. Paliwal, "Application of the spirometer in respiratory gated radiotherapy," Med. Phys. **30**, 3165–3171 (2003).
[34]W. Lu, P. J. Parikh, I. M. El Naqa, M. M. Nystrom, J. P. Hubenschmidt, S. H. Wahab, S. Mutic, A. K. Singh, G. E. Christensen, J. D. Bradley, and D. A. Low, "Quantitation of the reconstruction quality of a four-dimensional computed tomography process for lung cancer patients," Med. Phys. **32**, 890–901 (2005).
[35]F. Madsen, "Validation of spirometer calibration syringes," Scand. J. Clin. Lab. Invest. **72**, 608–613 (2012).
[36]T. Zhang, N. P. Orton, T. R. Mackie, and B. R. Paliwal, "Technical note: A novel boundary condition using contact elements for finite element based deformable image registration," Med. Phys. **31**, 2412–2415 (2004).
[37]L. I. Cervino, A. K. Chao, A. Sandhu, and S. B. Jiang, "The diaphragm as an anatomic surrogate for lung tumor motion," Phys. Med. Biol. **54**, 3529–3541 (2009).
[38]J. Yang, J. Cai, H. Wang, Z. Chang, B. G. Czito, M. R. Bashir, M. Palta, and F. F. Yin, "Is diaphragm motion a good surrogate for liver tumor motion?," Int. J. Radiat. Oncol., Biol., Phys. **90**, 952–958 (2014).
[39]J. E. McNamara, R. Regmi, D. Michael Lovelock, E. D. Yorke, K. A. Goodman, A. Rimner, H. Mostafavi, and G. S. Mageras, "Toward correcting drift in target position during radiotherapy via computer-controlled couch adjustments on a programmable Linac," Med. Phys. **40**, 051719 (5pp.) (2013).
[40]H. Yan, F. F. Yin, G. P. Zhu, M. Ajlouni, and J. H. Kim, "The correlation evaluation of a tumor tracking system using multiple external markers," Med. Phys. **33**, 4073–4084 (2006).
[41]J. D. Hoisak, K. E. Sixel, R. Tirona, P. C. Cheung, and J. P. Pignol, "Prediction of lung tumour position based on spirometry and on abdominal displacement: Accuracy and reproducibility," Radiother. Oncol. **78**, 339–346 (2006).
[42]G. Li, H. Xie, H. Ning, J. Capala, B. C. Arora, C. N. Coleman, K. Camphausen, and R. W. Miller, "A novel 3D volumetric voxel registration technique for volume-view-guided image registration of multiple imaging modalities," Int. J. Radiat. Oncol., Biol., Phys. **63**, 261–273 (2005).
[43]X. Jia, P. Ziegenhein, and S. B. Jiang, "GPU-based high-performance computing for radiation therapy," Phys. Med. Biol. **59**, R151–R182 (2014).
[44]R. Li, J. H. Lewis, X. Jia, X. Gu, M. Folkerts, C. Men, W. Y. Song, and S. B. Jiang, "3D tumor localization through real-time volumetric x-ray imaging for lung cancer radiotherapy," Med. Phys. **38**, 2783–2794 (2011).